

1 **A GCM Comparison of Plio-Pleistocene SuperInterglacial Periods in**
2 **Relation to Lake El'gygytgyn, NE Arctic Russia**

3

4 Anthony J. Coletti¹, Robert M. DeConto¹, Julie Brigham-Grette¹, Martin Melles²

5

6 [1] Department of Geosciences, University of Massachusetts, Amherst, MA, 01003, USA

7 [2] Institute of Geology and Mineralogy, University of Cologne, Zuelpicher Strasse 49a, D-

8 50674 Cologne, Germany

9

10

11 **Abstract**

12

13 **Until now, the lack of time-continuous, terrestrial paleoenvironmental data**
14 **from the Pleistocene Arctic has made model simulations of past interglacials**
15 **difficult to assess. Here, we compare climate simulations of four warm interglacials**
16 **at Marine Isotope Stage (MIS) 1 (9ka), 5e (127 ka), 11c (409 ka), and 31 (1072 ka)**
17 **with new proxy climate data recovered from Lake El'gygytgyn, NE Russia. Climate**
18 **reconstructions of the Mean Temperature of the Warmest Month (MTWM) indicate**
19 **conditions up to 0.4, 2.1, 0.5 and 3.1 °C warmer than today during MIS-1, 5e, 11c,**
20 **and 31, respectively. While the climate model captures much of the observed**
21 **warming during each interglacial, largely in response to boreal summer orbital**
22 **forcing, the extraordinary warmth of MIS-11c relative to the other interglacials in**
23 **the Lake El'gygytgyn temperature proxy reconstructions remains difficult to**
24 **explain. To deconvolve the contribution of multiple influences on interglacial**
25 **warming at Lake El'gygytgyn, we isolated the influence of vegetation, sea ice, and**
26 **circum-Arctic land ice feedbacks on the modeled climate of the Beringian interior.**
27 **Simulations accounting for climate-vegetation-land surface feedbacks during all**
28 **four interglacials show expanding boreal forest cover with increasing summer**
29 **insolation intensity. A deglaciated Greenland is shown to have a minimal effect on**
30 **Northeast Asian temperature during the warmth of stage 11c and 31 (Melles et al.,**
31 **2012). A prescribed enhancement of oceanic heat transport into the Arctic Ocean**

32 **does have some effect on Lake El'gygytgyn regional climate, but the exceptional**
33 **warmth of MIS-11c remains enigmatic relative to the modest orbital and greenhouse**
34 **gas forcing during that interglacial.**

35

36

37 **1. Introduction**

38

39 Knowledge of Pleistocene climate history has increased dramatically over the past
40 three decades, however existing records remain strongly biased toward an oceanic
41 viewpoint, due to the lack of long terrestrial archives. In the context of future warming, it
42 is clearly important to understand the effects of warming on the terrestrial Arctic, the
43 strength of polar amplification, and systemic teleconnections to and from other latitudes.
44 Past warm periods known as Interglacials, over the past 2.8 million years, provide a
45 means of studying climates warmer than today.

46 In 2009, a multinational team drilled a sediment core from a 25 km wide impact
47 crater lake named "Lake El'gygytgyn" (alternatively, Lake "E"), in northeast Siberia
48 (Brigham-Grette et al., 2013; Melles et al., 2012). The core contains the longest Arctic
49 terrestrial record ever recovered, extending back ~3.5 million years, and provides
50 evidence for periods of exceptional warmth during Pleistocene interglacials as defined by
51 marine benthic $\delta^{18}\text{O}$ records (Lisiecki and Raymo, 2005) (Figure 5A&B). It has been
52 shown that Marine Isotope Stage(s) 1, 5e, 11c and 31 were among the warmest
53 interglacials in the Pleistocene Arctic (Melles et al., 2012).

54 To explore the sensitivity of northwestern Beringia to interglacial forcing and the
55 mechanisms responsible for the observed climate changes, we use a Global Climate
56 Model coupled to an interactive vegetation model to simulate the terrestrial Arctic's
57 response to the greenhouse gas and astronomical forcing associated with specific
58 interglacial (e.g., Yin and Berger, 2011). A range of sensitivity tests were performed and
59 a range of changes in boundary conditions are imposed to test the response of the region
60 to changes in circum-Arctic ice sheets and possible changes of ocean heat transport into
61 the Arctic Ocean. The results are then compared to the Lake E multi-proxy
62 reconstructions.

63 2. Model and experimental design

64

65 All global climate simulations discussed herein were performed using the current
66 version of the Global ENvironmental and Ecological Simulation of Interactive Systems
67 (GENESIS) Global Climate Model (GCM) version 3.0 (Alder et al., 2011; Thompson and
68 Pollard, 1997). GENESIS is an atmosphere, land-surface, ocean, snow, sea ice, ice sheet
69 and vegetation coupled model. As used here, spectral resolution of the atmosphere GCM
70 is T31 resolution (approximately 3.75° resolution) with 18 vertical levels (Thompson and
71 Pollard, 1997). The AGCM is coupled to 2°x2° soil, snow, vegetation, ocean, and sea ice
72 model components. The GCM is interactively coupled to the BIOME4 (Kaplan, 2003)
73 vegetation model that predicts equilibrium vegetation distribution, structure and
74 biogeochemistry using monthly mean climatologies of precipitation, temperature and
75 clouds simulated by the GCM. Vegetation distributions take the form of 27 plant biomes
76 including 12 plant functional types (PFTs) that represent broad, physiologically distinct
77 classes (Kaplan, 2003). GENESIS includes options for coupling to an Ocean General
78 Circulation Model (Alder et al., 2011) or a non-dynamical, slab ocean model that
79 incorporates heat transfer, calculations of sea-surface temperatures (SST) and feedbacks
80 operating between ocean surface and sea ice. The slab mixed layer ocean model is used
81 here to allow multiple simulations to be performed with and without imposed
82 perturbations of surface ocean conditions. This version of the GCM has a sensitivity of
83 2.9 °C, without GHG, vegetation or ice sheet feedbacks. Greenhouse gasses and orbital
84 parameters for each interglacial simulation were prescribed according to ice core records
85 (Loulergue et al., 2008; Lüthi et al., 2008; Schilt et al., 2010) and standard astronomical
86 solutions (Berger, 1978).

87 The strategy adopted here was to target Marine Isotope Stage (MIS) 1 (11 ka), 5e
88 (127 ka), 11c (409 ka) and 31 (1072 ka), corresponding to the timing of peak summer
89 warmth observed at Lake E and identified as “super-interglacials” by Melles et al.,
90 (2012). Equilibrium simulations were performed at the time of peak boreal summer
91 insolation at 67.5°N (Laskar et al., 2004) assuming the real climate system equilibrated
92 within a half-precession cycle. Model temperature and precipitation values were
93 calculated from 20-year averages taken from the 60 to 80-year equilibrated simulations.

94 Preliminary analysis of pollen assemblages in the Lake E core is assumed to provide a
95 record of peak summer temperatures, so our data-model comparisons focus on warmest
96 monthly mean climate (July). A simulation of pre-industrial climate (280 ppmv $p\text{CO}_2$)
97 was run as a control experiment to evaluate the model's representation of Beringian
98 climate and to provide a baseline for comparing super-interglacial simulations. A modern
99 Greenland Ice Sheet (GIS) is prescribed unless otherwise noted. In simulations without a
100 GIS, the ice sheet is replaced with ice-free, isostatically equilibrated land surface
101 elevations.

102

103 **2.1 MIS 1, 9 ka**

104

105 MIS-1 represents the last 11,000 years and its onset roughly coincides with the
106 end of the Younger-Dryas (~11,500 ka). Peak boreal summer insolation occurs ~9 ka,
107 when summer insolation was $\sim 510 \text{ Wm}^{-2}$ at 65 °N, relative to 446 Wm^{-2} today. Proxy
108 indicators suggest conditions were warmer than present (+1.6 °C over western Arctic and
109 +2 to 4°C in circum-Arctic) with lush birch and alder shrubs (Melles et al., 2012)
110 dominating the vegetation around the lake. This period, known as the Holocene Climate
111 Optimum (HCO), was spatially variable, with most warming in the high latitudes, and
112 minimal warming in the mid-latitudes and tropics (Kitoh and Murakami, 2002).

113

114 **2.2 MIS-5e, 127 ka**

115 MIS-5e, also known as the Last InterGlaciation (LIG), is one of the warmest
116 interglacials of the Pleistocene and lasted roughly ~12-10 kyr (130 to 116 ka). High
117 obliquity, eccentricity and the timing of perihelion (precession) combined to produce
118 high intensity boreal summer insolation at around 127 ka. Greenland ice core records
119 (Dahl-Jensen and NEEM community members, 2013) suggest summer warming up to
120 8 ± 4 °C over northeast Greenland, but only a modest reduction in the size of the
121 Greenland Ice Sheet (GIS). Studies involving Sr – Nd – Pb isotope ratios of silt-sized
122 sediment discharged from southern Greenland suggest that no single southern Greenland
123 geologic terrain was completely deglaciated during the LIG, however, some southern GIS
124 retreat was evident (Colville et al., 2011). A previous model study of MIS-5e by (Yin and

125 Berger, 2011) involved running a model of intermediate complexity to test relative
126 contributions of Greenhouse Gas (GHG) and insolation forcing on LIG warmth. They
127 found that GHGs play a dominant role on the variations of the annual mean temperature
128 of both the globe and the southern high latitudes, whereas, insolation plays a dominant
129 role on precipitation, northern high latitude temperatures, and sea ice extent (Yin and
130 Berger, 2011). Similarly, model simulations have shown that insolation anomalies during
131 MIS-5e likely caused significant summer (JJA) warming throughout the Arctic (Bakker
132 et al., 2013; Lunt et al., 2013; Otto-Bliesner et al., 2006).

133 The LIG simulation shown here is used to compare paleoenvironmental
134 conditions in western Beringia, including, temperature, vegetation and precipitation, to
135 Lake E pollen proxy analysis. Orbital parameters and greenhouse gas concentrations are
136 set at their 127 ka values to represent peak boreal warmth during MIS-5e.

137

138 **2.3 MIS-11c, 409 kyr**

139

140 MIS-11c is another exceptionally warm interglacial (Howard, 1997) that lasted
141 from 428 to 383 ka (~45 ka). Sediment records from the Arctic containing information on
142 MIS-11 are generally lacking (Miller et al., 2010b). Unlike the other interglacials, MIS-
143 11c was remarkably long, with two boreal insolation maxima at ~409 ka and 423 ka,
144 creating extensive warmth throughout the Arctic (Melles et al., 2012). Unlike MIS-5e,
145 there is evidence that the GIS may have been much reduced in size (Raymo and
146 Mitrovica, 2012; Willerslev et al., 2007), with lush boreal forest covering most of
147 southern Greenland (de Vernal and Hillaire-Marcel, 2008). Particularly warm conditions
148 are also suggested by pollen records analyzed from Lake Biwa (Tarasov et al., 2011)
149 located in Shiga Prefecture, Japan. Likewise, a study from Lake Baikal also indicates
150 warmer than modern temperatures with a “conifer optimum” suggesting warmer
151 conditions and less aridity, perhaps influenced by higher sea levels and reduced
152 continentality (Prokopenko et al., 2010).

153 Three different simulations (Table 1, 2) were run to test the sensitivity of the lake
154 region to MIS-11c forcing. The first simulation uses default boundary conditions,
155 including a modern GIS (MIS11GIS). The second simulation tests the sensitivity of the

156 Lake E region to an ice-free Greenland (MIS11NG). In this simulation, the entire GIS
157 was removed and topography of Greenland was corrected for glacial isostatic adjustment.
158 The final sensitivity experiment includes an increase in sub-sea ice surface heat flux from
159 2 Wm^2 in our modern control, to 10 Wm^2 (additional $+8 \text{ Wm}^2$) to test the Beringian
160 sensitivity to a mostly ice-free Arctic Ocean. The increased heat flux assumes an extreme
161 ~ 3 Sverdrup (Sv) increase in Bering Strait through flow and a $4 \text{ }^\circ\text{C}$ temperature contrast
162 between North Pacific and North Polar surface water (Melles et al., 2012, supplemental).
163 The additional heat flux convergence is used to crudely mimic the influence of a wider
164 and deeper Bering Strait during times of higher sea level. Using the predictive BIOME4
165 interactive vegetation model, direct comparisons of observed and modeled Arctic
166 vegetation within the Lake E region can be made. Furthermore, simulations using
167 prescribed distributions of biome flora can be used to quantify the local effect of
168 changing vegetation cover around the region.

169

170 **2.4 MIS-31, 1072 ka**

171

172 MIS-31 (~ 1062 - 1082 ka) (Lisiecki and Raymo, 2005) has only been identified in
173 a few Arctic records prior to Lake E. The Interglacial represents one of the last 41-kyr
174 glacial cycles and is best known for extreme warmth in circum-Antarctica ocean waters
175 induced by a deterioration of the Polar Front (Scherer et al., 2008) and the collapse of the
176 marine based West Antarctic Ice Sheet (WAIS) (DeConto et al., 2012; Pollard &
177 DeConto, 2009), by intrusion of warm surface waters onto Antarctic continental shelves.
178 On Ellesmere Island, Fosheim Dome includes terrestrial deposits that date to ~ 1.1 Ma,
179 which contains fossil beetle assemblages dated within MIS-31, suggesting temperatures
180 of 8 to $14 \text{ }^\circ\text{C}$ above modern values (Elias and Matthews Jr., 2002). It is speculated, like
181 MIS-11c, that the Arctic may have been too warm to support a GIS which may have been
182 substantially reduced in size, or possibly nonexistent (Melles et al., 2012; Raymo and
183 Mitrovica, 2012). Therefore, simulations of MIS-31 are run both with and without a GIS
184 (Table 1, 2).

185

186

187 **3. Results**

188 **3.1 Control Simulations**

189 **3.1.1 Pre-Industrial**

190

191 Simulations of preindustrial 2-m mean annual temperature (MAAT) and MTWM
192 at Lake E are -12 and 10.3 °C respectively, -3 °C and -1.7 °C lower than the modern
193 simulations. Preindustrial summer temperatures (8 °C) are -2.2 °C lower than modern.
194 GHG radiative forcing from a combination of CO₂, CH₄, and N₂O atmospheric mixing
195 ratios implies a 1.8 Wm⁻² reduction relative to modern, accounting for most of the cooling
196 in the preindustrial simulation. Generally, mean annual precipitation (PANN) values in
197 the cooler, preindustrial simulation are slightly lower than modern precipitation. At Lake
198 E, preindustrial annual precipitation was 438 mm year⁻¹, substantially wetter than
199 observations (+122 mm year⁻¹). Winter (DJF) precipitation in the preindustrial simulation
200 was ~24 mm month⁻¹, while mean summer (JJA) precipitation was 43 mm month⁻¹.

201 Simulated pre-industrial vegetation distributions are assumed to be in equilibrium
202 (Fig. 3A). In the preindustrial simulation, shrub tundra dominates the Lake E region, with
203 evergreen taiga and deciduous forests maintained in interior Siberia and Yukon.
204 Simulated Siberian biome distributions are similar to modern day vegetation described by
205 Kolosova (1980) and Viereck & Little Jr (1975). Shrub tundra in the preindustrial
206 simulation can be attributed to cool and dry Arctic conditions in the preindustrial run.

207

208 **3.2 Paleoclimate simulations**

209 **3.2.1 MIS-1 (9 ka); Holocene Thermal Maximum**

210

211 July temperatures at Lake E in the MIS-1 simulation (12.4 °C) are ~2.1 °C
212 warmer than preindustrial (10.3 °C) and summer (JJA) temperatures are 1.6 °C warmer
213 (Fig. 2A). Overall, the Siberian interior warms > 5 °C in July, relative to preindustrial.
214 Simulated MTWM exceed > 2 °C around Lake E.

215 Simulated MIS-1 PANN values at the lake (~438 mm year⁻¹) are close to
216 preindustrial values, although somewhat drier conditions dominate further inland,
217 possibly as a result attributed increased proximity away from a moisture source.

218 Simulated vegetation around Lake E is close to the transition between dominant shrub
219 tundra to the east and deciduous forest to the west (Fig. 3B).

220

221 **3.2.2 MIS-5e (127 ka)**

222

223 Overall warming of the Beringian interior in the MIS-5e simulation is > 2 °C
224 relative to preindustrial temperatures (Fig. 2B). Most of this warming can be attributed to
225 the direct effects of the MIS-5e orbit (Groll et al., 2005; Langebroek and Nisancioglu,
226 2014), which produces an Arctic summer insolation anomaly of >50 Wm^{-2} at the top of
227 the atmosphere, relative to a pre-industrial (modern) orbit (Fig. 1B). According to ice
228 core records, carbon dioxide (CO_2) concentrations during this period were about 287
229 ppmv, contributing 0.132 Wm^{-2} more surface radiative forcing than preindustrial, but the
230 combination of CO_2 , CH_4 , and N_2O attributes just -0.0035 Wm^{-2} forcing relative to
231 preindustrial GHG mixing ratios.

232 Comparing MIS-5e with respect to the preindustrial control simulation at Lake E
233 shows differences in summer (JJA) and MTWM temperatures of $+2.5$ and $+4.2$ °C,
234 respectively (Fig. 2B). Summer warming over the GIS is $+5$ °C relative to preindustrial,
235 which is comparable to the LIG warming reported in a recent Greenland ice core study
236 (Dahl-Jensen and NEEM community members, 2013). Mean annual precipitation at Lake
237 E (~ 401 mm year^{-1}), is 37 mm year^{-1} less than pre-industrial levels, and the difference is
238 statistically significant at the 95% confidence level with a p-value of 0.029. Overall,
239 similar precipitation patterns are seen at Lake E, relative to MIS-5e and the pre-industrial
240 control scenario, which reflects both the overall wet bias in the GCM and the similar
241 continental/ice sheet boundary conditions, in both simulations.

242 A less moist, but warm high latitude environment produces deciduous taiga and
243 evergreen taiga biome distributions around Lake E (Fig. 3C), with evergreen taiga being
244 the most dominant in eastern Beringia and deciduous taiga being more dominant around
245 the Lake E region and most of western Beringia.

246

247 **3.2.3 MIS-11c (409 ka)**

248

249 Due to an eccentricity minimum, MIS-11c is a longer interglacial than the other
250 interglacials in this study (Howard, 1997). We assume an ice-free Greenland in our MIS-
251 11c simulations, with the ice sheet removed and replaced with isostatically equilibrated
252 (ice-free) land elevations. Additional experiments including an imposed increase in sub-
253 sea ice heat flux in the Arctic Ocean basin will also be discussed.

254 Model simulations show summer insolation anomalies (relative to preindustrial)
255 during MIS-11c ranging from $+45 - 55 \text{ Wm}^{-2}$ (Fig. 1C) allowing temperatures over the
256 Lake E region during July (month of maximum insolation) to increase $2.2 \text{ }^\circ\text{C}$ relative to
257 preindustrial. Overall, mean annual summer temperatures (JJA) over the circum-Arctic
258 and Lake E are 2 to $4 \text{ }^\circ\text{C}$ warmer than pre-industrial temperatures, with the Siberian
259 interior warming the most (Table 2).

260 In MIS-11c simulations performed with (MIS11GIS) and without a GIS
261 (MIS11NG), the effect on temperature at the Lake E is shown to be small ($\sim 0.3 \text{ }^\circ\text{C}$).
262 Geopotential height anomalies at 500hPa ($+4 - 10$ meters) indicate upper-level warming
263 east of Lake E, and cooling west of Lake E, but the net effect of ice sheet loss on surface
264 air temperatures is mostly limited to Greenland itself and the proximal ocean, with little
265 effect at the distance of Lake E, as shown in other modeling studies (Koenig et al., 2012;
266 Otto-Bliesner et al., 2006).

267 The warmer MIS-11c climate and possible reductions of Greenland and West
268 Antarctic ice sheet sheets are thought to have contributed to sea levels as much as >11
269 meters (Raymo and Mitrovica, 2012) higher than today. Arctic sea ice was also possibly
270 reduced (Cronin et al., 2013; Polyak et al., 2010). In order to test the influence of high
271 sea levels and a mostly ice-free Arctic Ocean on Lake E climate, heat flux convergence
272 under sea ice was increased from 2 Wm^{-2} to 10 Wm^{-2} in the slab ocean/dynamic sea ice
273 model. The resulting reductions in sea ice extent and warmer ($\sim 0.2 - 1.0 \text{ }^\circ\text{C}$) (Fig. 4A)
274 Arctic SST's produced negligible warming around Lake E ($< 0.7 \text{ }^\circ\text{C}$), suggesting the
275 Lake E region was relatively insensitive to Arctic Ocean conditions.

276 Precipitation amounts at Lake E during MIS11GIS are close to modern values of
277 475 mm year^{-1} . Also, MIS11NG exhibits the same precipitation amounts as our pre-
278 industrial control run ($\sim 438 \text{ mm year}^{-1}$) (Table 2). Simulated precipitation conditions in
279 the Arctic Ocean basin are fairly dry, $\sim 200 \text{ mm year}^{-1}$, comparable to reanalysis data sets

280 (Serreze and Hurst, 2000). On the contrary, simulations of MIS11NG show reduced
281 precipitation amounts by -37 mm year^{-1} relative to MIS11GIS. Runs with increased sub-
282 ice oceanic heat flux reduced the drying seen in the MIS11NG simulation and produced
283 values matching rainfall rates of modern control values ($\sim 475 \text{ mm year}^{-1}$).

284 A warmer and wetter MIS-11c places Lake E on the border of evergreen taiga and
285 shrub tundra biomes (Fig. 3D). Vegetation limits, such as tree lines, are slightly changed
286 during our simulations with increased heat flux and a warmer, open Arctic Ocean.
287 Evergreen forests around the Lake E region extend poleward to the coast and slightly
288 eastward.

289

290 **3.2.4 MIS-31 (1072 ka)**

291

292 An extreme warm orbit with high obliquity, high eccentricity and precession
293 aligning perihelion with boreal summer allows insolation anomalies to be $> 50 \text{ Wm}^{-2}$ at
294 the surface and $+ 60 - 80 \text{ W m}^{-2}$ (Fig. 1D) at the top of the atmosphere at the latitude of
295 Lake E. Average summer temperatures around the lake are about $+3.6 \text{ }^{\circ}\text{C}$ warmer than
296 preindustrial (Fig. 2D; Table 2). While MIS-31 is beyond the temporal range of ice core
297 greenhouse gas records, proxy geochemical records imply MIS-31 has the highest $p\text{CO}_2$
298 ($\sim 325 \text{ ppmv}$) of the mid-Pleistocene (Hönisch et al., 2009), contributing $\sim +0.80 \text{ Wm}^{-2}$
299 relative to pre-industrial values. As a result, modeled July temperatures at Lake E are >5
300 $^{\circ}\text{C}$ warmer than pre-industrial temperatures.

301 Simulated precipitation at Lake E during MIS-31 is $\sim 438 \text{ mm year}^{-1}$ (Table 2),
302 similar to that in MIS-11c simulations. Vegetation distribution is similar to the other
303 interglacials described here (Fig. 3E). The Lake E region is dominated by evergreen
304 taiga.

305

306 **4. Discussion**

307

308 The warm periods of Marine Isotope Stage(s) 1, 5e, 11c and 31 show similar
309 changes around Lake E. Temperature reconstructions during the Holocene Thermal
310 Maximum (9 kyr) indicate $+1.6 (\pm 0.8) \text{ }^{\circ}\text{C}$ warming in the western Arctic (Kaufman and

311 Brigham-Grette, 1993) with an overall warming of 1.7 (± 0.8) °C in the circum-Arctic
312 (Miller et al., 2010a), relative to modern temperatures. Though our model does not fully
313 account for all the warming during this period, it does produce the warming in the
314 western Arctic as documented by Kaufman and Brigham-Grette (1993). With the
315 decrease in Arctic moisture and low CO₂, deciduous and evergreen forests dominate the
316 Arctic in the model, matching the dominant vegetation such as *Alnus*, *Betula* (nut bearing
317 trees and fruits), *Poaceae* (grasses) and some birch and alder seen in the Lake E record
318 (Melles et al., 2012).

319 Marine Isotope Stage 5e produced the greatest summer warming among the four
320 interglacials simulated here. Comparisons with a preindustrial control run show that
321 differences in MTWM at Lake E during MIS-1 and 5e (+2.1 and +4.2 °C) are similar to
322 the changes seen in MIS11NG and 31(+2.2 and +3.5 °C) (Table 2). Similar warming has
323 been seen in other modeling studies showing that a high obliquity and high eccentricity
324 with precession aligning perihelion with boreal summer will yield the warmest boreal
325 summer temperatures (Koenig et al., 2011; Lunt et al., 2013; Otto-Bliesner et al., 2006;
326 Yin and Berger, 2011). Strong insolation forcing at these latitudes cause July maximum
327 temperatures to exceed pre-industrial temperatures by >2 °C. The 2–4 °C simulated MIS-
328 5e warming in Siberia and Lake E has also been seen in proxy data compilations (CAPE,
329 2006; Lozhkin and Anderson (1995); Lozhkin et al. (2006)) and in simulations using a
330 GCM without vegetation feedbacks. Most of the warming has been linked to the summer
331 insolation anomaly associated with the MIS-5e orbit (Otto-Bliesner et al., 2006). The
332 exceptional summer warmth of MIS-5e compared to other interglacials was previously
333 thought to have caused a substantial reduction in the GIS, however, more recent work
334 suggests the GIS contributed only ~1.4 to 4.3 m of equivalent eustatic sea level rise
335 during the LIG (Colville et al., 2011; Quiquet et al., 2013; Robinson et al., 2011; Stocker
336 et al., 2013; Stone et al., 2013), and remained mostly intact (Dahl-Jensen and NEEM
337 community members, 2013). This suggests that our simulations of MIS-5e with a modern
338 GIS are a good approximation for this period. Colder and fresher sea surface conditions
339 in the North Atlantic, Labrador and Norwegian Seas have been found in marine
340 sediments records possibly indicating freshwater input (perhaps from parts of Greenland)
341 which may have led to early LIG warming attributed to stronger ocean overturning

342 (Govin et al., 2012). In the model, Arctic warming during MIS-5e allows almost a full
343 replacement of shrub tundra with deciduous forest in and around the Lake E region.
344 Pollen analysis during this period shows tree species of birch, alder, pine and spruce
345 (Melles et al., 2012). However, multiproxy studies of MIS-5e show a change in MTWM
346 of only +2 °C compared to modern temperatures (Melles et al., 2012) (Table 2). It can be
347 concluded that the warm boreal summer orbit at MIS-5e can account for much of the
348 warmth in Beringia, and the cirum-Arctic, but the particularly muted response in the Lake
349 E proxy record to summer insolation forcing cannot be fully explained.

350 Simulations of MIS-11c exhibit another very warm interglacial at Lake E, with
351 MTWM maxima approaching +2.2 °C warmer than pre-industrial temperatures (Table 2).
352 Similarly to MIS-5e and 1, peak warmth coincides with perihelion during boreal summer,
353 however low eccentricity and obliquity attenuates the effects of precession relative to 5e
354 and 1, making summer insolation less intense. A combination of eccentricity, obliquity
355 and precession elevates summer insolation for ~45k years, a much longer (but less
356 intense) interval of elevated summer insolation than during the other interglacials studied
357 here. The overall warmth of MIS-11 is, in part, an outcome of reduced snow and ice
358 cover.

359 Another possible mechanism contributing to Lake E warmth at MIS-11 might be
360 related to elevated sea level at this time (Raymo and Mitrovica, 2012), possibly
361 contributing to increased Bering Strait throughflow. Today, the Bering Strait is limited to
362 ~50 m in depth with a net northward transport of ~0.8 Sv (Woodgate et al., 2010).
363 Oceanic heat transport into the Arctic basin might have been elevated during high sea
364 level, providing a source of warm water intrusion into the Arctic Ocean basin from the
365 North Pacific. As a simple test of the potential for a warmer Arctic Ocean with less sea
366 ice to affect temperatures over terrestrial Beringia, heat flux convergence under sea ice in
367 the Arctic Ocean was increased from 2 to 10 W m⁻². Summer sea ice fraction was
368 reduced by 25 – 50 % and summer ocean temperatures warmed by 0.2 – 1.0 °C (Fig.
369 4A,B). The warmer Arctic Ocean warmed the Lake E region, but only slightly (+0.7 °C),
370 and does not account for the exceptional warmth observed during MIS-11c relative to
371 MIS-5e.

372 The influence of MIS-11c temperatures on terrestrial biome distributions is
373 supported by a poleward advance of evergreen needle-leaf forest around the lake, which
374 is in good agreement with palynological analysis (Melles et al., 2012) showing forest-
375 tundra and northern larch-taiga dominated by spruce, pine, birch, alder and larch (Melles
376 et al., 2012). Surface warming as a result of albedo feedbacks associated with needle-leaf
377 forests during snow-covered months accounts for some of the warming during this
378 period, however increased evergreen, terrestrial forest and enhanced evapotranspiration
379 provides a slight net cooling during the summers.

380 A deglaciated Greenland has been shown to have regional effects on SSTs and
381 sea-ice conditions, however warming of the circum-Arctic has been shown to be minimal
382 (Koenig et al., 2012; Otto-Bliesner et al., 2006). This is also demonstrated in our
383 simulations, whereby the loss of the GIS warms summer annual temperatures around
384 Lake E by only 0.3 °C (Table 2). An analysis of 500 hPa geopotential height anomalies
385 show ridging (positive height anomalies of > 10 m) to the east and troughing (negative
386 height anomalies) to the west of Lake E, indicating a slight change in the large-scale
387 planetary wave patterns over Beringia. Over Lake E, positive height anomalies are also
388 present, indicating slightly warmer conditions and a slight eastward shift of an
389 atmospheric ridge that may have been set up further west of Lake E. The ridging in these
390 simulations may also be related to a decrease in precipitation at Lake E when the GIS is
391 removed in GCM. Extended high pressure over Beringia associated with ridging would
392 create somewhat drier conditions for the region. If the exceptional warmth of MIS-11c is
393 indeed related to the melting of the GIS, freshwater input may have been a mechanism to
394 strengthen North Atlantic overturning creating the warmth missing in our simulations
395 (Govin et al., 2012). Furthermore, it is not clear why the GIS would have survived MIS-
396 5e warmth, and not MIS-11c. In sum, the exceptional Arctic warmth of MIS-11c remains
397 difficult to explain and is not a straightforward result of greenhouse gases, orbital forcing,
398 vegetation feedbacks, or Arctic Ocean warming.

399 Elevated GHG concentrations and a very warm summer orbit can explain much of
400 the warmth during MIS-31, assuming atmospheric CO₂ was higher than MIS-5e and
401 MIS-11 (Hönisch et al., 2009). In the model, the combination of elevated greenhouse
402 gases and strong summer insolation forcing at 1072 ka allow dense needle-leaf and

403 deciduous forests to grow around the Lake. Simulated summer temperatures are about 12
404 °C (Table 2), +2 °C warmer than modern summer temperatures around Lake E. Biome
405 simulations derived from pollen analysis of the Lake E core show a maxima of trees and
406 shrubs during peak northern hemisphere insolation of MIS-31 at 1072 ka. Our model
407 simulations show similar results around Lake E, with increased boreal forest and less
408 tundra and small dwarf shrubs. The snow-albedo effect combined with low-albedo forest
409 cover allows temperatures to increase in the Arctic during MIS-31. Peak precipitation
410 rates derived from proxy analysis indicate about 600 mm year⁻¹, or about 125 mm year⁻¹
411 more precipitation than in our modern model simulation (Melles et al., 2012). GCM
412 results at MIS-31 indicate annual precipitation of ~490 mm year⁻¹ (Table 2), the most
413 annual precipitation among the four interglacials simulated here. While the GCM does
414 not fully capture the enhanced precipitation indicated in the proxy record, a relative
415 increase in precipitation is evident. Extraordinary warmth during MIS-31 correlates well
416 with a diminished WAIS (Pollard and DeConto, 2009) implying strong inter-hemispheric
417 coupling that has been related to possible reductions in Antarctic Bottom Water (AABW)
418 formation during times of ice-shelf retreat and increased fresh water input into the
419 Southern Ocean (Foldvik, 2004). WAIS collapse could also be linked with the Beringian
420 and Lake E warmth during MIS-11c and MIS-5e, but definitive evidence of WAIS retreat
421 during these later Pleistocene interglacials is currently lacking (McKay et al., 2012).

422

423

424 **5. Conclusions**

425

426 Lake E provides a high-resolution terrestrial proxy record of climate variability in
427 the Arctic. A linked climate modeling study described here shows that Arctic summers
428 were significantly warmer during several Pleistocene interglacials by as much as + 2 °C
429 during MIS-1 and 11c, and by as much as + 4 °C during MIS-5e and 31 relative to pre-
430 industrial. It can be inferred that most of the warming in the interglacial simulations can
431 be attributed to a combination of elevated GHGs and astronomical forcing, although,
432 astronomical forcing (at times producing high-intensity summer insolation >50 Wm⁻²
433 higher than today) was the dominant warming mechanism. Greenhouse gas levels during

434 MIS-31 remain poorly known, and the extreme warmth of this particular interglacial
435 could have been substantially augmented by GHG forcing. MIS-1 had relatively low CO₂
436 around the time of peak Holocene warmth, producing 0.44 Wm⁻² less radiative forcing
437 relative to pre-industrial levels (Melles et al., 2012), but the combination of orbital
438 forcing and perhaps other factors such as changes in Antarctic Bottom Water (AABW)
439 production and reduced Arctic sea-ice may have contributed to exceptional Arctic
440 warmth at this time. Thorough testing of these ideas will require additional simulations
441 with coupled atmosphere-ocean models, changes in circum-arctic ice sheets, eustatic sea-
442 levels, continentality, changes in sea-ice distributions and the addition of melt-water
443 inputs into northern and southern hemisphere oceans.

444 Extreme interglacial warmth shifted Lake E vegetation from mostly tundra with
445 small shrubs as we see the Arctic today to thick, lush evergreen and boreal forest. Due to
446 the extreme warmth, wetter conditions prevailed during the super-interglacials, allowing
447 forest biomes to thrive and increase their maximum extent poleward. While simulated
448 warming at Lake E is broadly similar during each interglacial, the vegetation response in
449 each simulation is unique, reflecting differences in seasonal temperatures and
450 hydroclimate. The GIS was significantly reduced during some interglacials (Stone et al.,
451 2013), allowing summer temperatures to increase to almost 16 °C warmer than present
452 over Greenland, but with limited impact on temperatures around Lake E. The observed
453 response of Beringia's climate and terrestrial vegetation to super-interglacial forcing is
454 still not fully understood and creates a challenge for climate modeling and for quantifying
455 the strength of Arctic amplification. Among the interglacials studied here, MIS-11c is the
456 warmest interglacial in the Lake E record, yet MIS-5e is the warmest simulated by the
457 model. The model produces overall drier conditions in the earlier interglacials (11c and
458 31) than suggested by pollen analysis. If the proxy interpretations were correct, this
459 would suggest that the model is missing some important regional processes. The timing
460 of significant warming in the circum-Arctic can be linked to major deglaciation events in
461 Antarctica, demonstrating possible inter-hemispheric linkages between the Arctic and
462 Antarctic climate on glacial-interglacial timescales, which have yet to be explained.

463

464

465 **References**

466

467 Alder, J. R., Hostetler, S. W., Pollard, D. and Schmittner, A.: Evaluation of a present-day
468 climate simulation with a new coupled atmosphere-ocean model GENMOM, *Geosci.*
469 *Model Dev.*, 4(1), 69–83, doi:10.5194/gmd-4-69-2011, 2011.

470 Bakker, P., Stone, E. J., Charbit, S., Gröger, M., Krebs-Kanzow, U., Ritz, S. P., Varma,
471 V., Khon, V., Lunt, D. J., Mikolajewicz, U., Prange, M., Renssen, H., Schneider, B. and
472 Schulz, M.: Last interglacial temperature evolution - a model inter-comparison, *Clim.*
473 *Past*, 9(2), 605–619, doi:10.5194/cp-9-605-2013, 2013.

474 Berger, A.: Long-Term Variations of Daily Insolation and Quaternary Climatic Changes,
475 *J. Atmospheric Sci.*, 35(12), 2362–2367, doi:10.1175/1520-
476 0469(1978)035<2362:LTVODI>2.0.CO;2, 1978.

477 Brigham-Grette, J., Melles, M., Minyuk, P., Andreev, A., Tarasov, P., DeConto, R.,
478 Koenig, S., Nowaczyk, N., Wennrich, V., Rosen, P., Haltia, E., Cook, T., Gebhardt, C.,
479 Meyer-Jacob, C., Snyder, J. and Herzschuh, U.: Pliocene Warmth, Polar Amplification,
480 and Stepped Pleistocene Cooling Recorded in NE Arctic Russia, *Science*, 340(6139),
481 1421–1427, doi:10.1126/science.1233137, 2013.

482 Colville, E. J., Carlson, A. E., Beard, B. L., Hatfield, R. G., Stoner, J. S., Reyes, A. V.
483 and Ullman, D. J.: Sr-Nd-Pb Isotope Evidence for Ice-Sheet Presence on Southern
484 Greenland During the Last Interglacial, *Science*, 333(6042), 620–623,
485 doi:10.1126/science.1204673, 2011.

486 Cronin, T. M., Polyak, L., Reed, D., Kandiano, E. S., Marzen, R. E. and Council, E. A.:
487 A 600-ka Arctic sea-ice record from Mendeleev Ridge based on ostracodes, *Sea Ice*
488 *Paleoclimate Syst. Chall. Reconstr. Sea Ice Proxies*, 79(0), 157–167,
489 doi:10.1016/j.quascirev.2012.12.010, 2013.

490 Dahl-Jensen, D. and NEEM community members: Eemian interglacial reconstructed
491 from a Greenland folded ice core, *Nature*, 493(7433), 489–494, doi:10.1038/nature11789,
492 2013.

493 DeConto, R. M., Galeotti, S., Pagani, M., Tracy, D., Schaefer, K., Zhang, T., Pollard, D.
494 and Beerling, D. J.: Past extreme warming events linked to massive carbon release from
495 thawing permafrost, *Nature*, 484(7392), 87–91, doi:10.1038/nature10929, 2012.

496 Elias, S. A. and Matthews Jr., J. V.: Arctic North American seasonal temperatures from
497 the latest Miocene to the Early Pleistocene, based on mutual climatic range analysis of
498 fossil beetle assemblages, *Can. J. Earth Sci.*, 39(6), 911–920, doi:10.1139/e01-096, 2002.

499 Foldvik, A.: Ice shelf water overflow and bottom water formation in the southern
500 Weddell Sea, *J. Geophys. Res.*, 109(C2), doi:10.1029/2003JC002008, 2004.

501 Govin, A., Braconnot, P., Capron, E., Cortijo, E., Duplessy, J.-C., Jansen, E., Labeyrie,
502 L., Landais, A., Marti, O., Michel, E., Mosquet, E., Risebrobakken, B., Swingedouw, D.
503 and Waelbroeck, C.: Persistent influence of ice sheet melting on high northern latitude
504 climate during the early Last Interglacial, *Clim. Past*, 8(2), 483–507, doi:10.5194/cp-8-
505 483-2012, 2012.

506 Groll, N., Widmann, M., Jones, J. M., Kaspar, F. and Lorenz, S. J.: Simulated
507 relationships between regional temperatures and large-scale circulation: 125 kyr BP
508 (Eemian) and the preindustrial period, *J. Clim.*, 18(19), 4032–4045, 2005.

509 Hönisch, B., Hemming, N. G., Archer, D., Siddall, M. and McManus, J. F.: Atmospheric
510 Carbon Dioxide Concentration Across the Mid-Pleistocene Transition, *Science*,
511 324(5934), 1551–1554, doi:10.1126/science.1171477, 2009.

512 Howard, W. R.: Palaeoclimatology: A warm future in the past, *Nature*, 388(6641), 418–
513 419, 1997.

514 Kaplan, J. O.: Climate change and Arctic ecosystems: 2. Modeling, paleodata-model
515 comparisons, and future projections, *J. Geophys. Res.*, 108(D19),
516 doi:10.1029/2002JD002559, 2003.

517 Kaufman, D. S. and Brigham-Grette, J.: Aminostratigraphic correlations and
518 paleotemperature implications, Pliocene-Pleistocene high-sea-level deposits,
519 northwestern Alaska, *Quat. Sci. Rev.*, 12(1), 21–33, doi:10.1016/0277-3791(93)90046-O,
520 1993.

521 Kitoh, A. and Murakami, S.: Tropical Pacific climate at the mid-Holocene and the Last
522 Glacial Maximum simulated by a coupled ocean-atmosphere general circulation model,
523 *Paleoceanography*, 17(3), 19–1–19–13, doi:10.1029/2001PA000724, 2002.

524 Koenig, S. J., DeConto, R. M. and Pollard, D.: Late Pliocene to Pleistocene sensitivity of
525 the Greenland Ice Sheet in response to external forcing and internal feedbacks, *Clim.*
526 *Dyn.*, 37(5-6), 1247–1268, doi:10.1007/s00382-011-1050-0, 2011.

527 Koenig, S. J., DeConto, R. M. and Pollard, D.: Pliocene Model Intercomparison Project
528 Experiment 1: implementation strategy and mid-Pliocene global climatology using
529 GENESIS v3.0 GCM, *Geosci. Model Dev.*, 5(1), 73–85, doi:10.5194/gmd-5-73-2012,
530 2012.

531 Kolosova, L.: *Geographical Atlas*, 1980.

532 Langebroek, P. M. and Nisancioglu, K. H.: Simulating last interglacial climate with
533 NorESM: role of insolation and greenhouse gases in the timing of peak warmth, *Clim.*
534 *Past*, 10(4), 1305–1318, doi:10.5194/cp-10-1305-2014, 2014.

535 Laskar, J., Robutel, P., Joutel, F., Gastineau, M., Correia, A. C. M. and Levrard, B.: A
536 long-term numerical solution for the insolation quantities of the Earth, *Astron.*

- 537 Astrophys., 428(1), 261–285, doi:DOI: <http://dx.doi.org/10.1051/0004-6361:20041335>,
538 2004.
- 539 Lisiecki, L. E. and Raymo, M. E.: A Pliocene-Pleistocene stack of 57 globally distributed
540 benthic $\delta^{18}\text{O}$ records, *Paleoceanography*, 20(1), PA1003, doi:10.1029/2004PA001071,
541 2005.
- 542 Loulergue, L., Schilt, A., Spahni, R., Masson-Delmotte, V., Blunier, T., Lemieux, B.,
543 Barnola, J.-M., Raynaud, D., Stocker, T. F. and Chappellaz, J.: Orbital and millennial-
544 scale features of atmospheric CH_4 over the past 800,000 years, *Nature*, 453(7193), 383–
545 386, doi:10.1038/nature06950, 2008.
- 546 Lozhkin, A. V. and Anderson, P. M.: The Last Interglaciation in Northeast Siberia,
547 *Quaternary Research*, 43, 147–158, 1995.
- 548 Lozhkin, A. V., Anderson, P. M., Matrosova, T. V. and Minyuk, P. S.: The pollen record
549 from El'gygytgyn Lake: implications for vegetation and climate histories of northern
550 Chukotka since the late middle Pleistocene, *J. Paleolimnol.*, 37(1), 135–153,
551 doi:10.1007/s10933-006-9018-5, 2006.
- 552 Lunt, D. J., Abe-Ouchi, A., Bakker, P., Berger, A., Braconnot, P., Charbit, S., Fischer, N.,
553 Herold, N., Jungclaus, J. H., Khon, V. C., Krebs-Kanzow, U., Langebroek, P. M.,
554 Lohmann, G., Nisancioglu, K. H., Otto-Bliesner, B. L., Park, W., Pfeiffer, M., Phipps, S.
555 J., Prange, M., Rachmayani, R., Renssen, H., Rosenbloom, N., Schneider, B., Stone, E. J.,
556 Takahashi, K., Wei, W., Yin, Q. and Zhang, Z. S.: A multi-model assessment of last
557 interglacial temperatures, *Clim Past*, 9(2), 699–717, doi:10.5194/cp-9-699-2013, 2013.
- 558 Lüthi, D., Le Floch, M., Bereiter, B., Blunier, T., Barnola, J.-M., Siegenthaler, U.,
559 Raynaud, D., Jouzel, J., Fischer, H., Kawamura, K. and Stocker, T. F.: High-resolution
560 carbon dioxide concentration record 650,000–800,000 years before present, *Nature*,
561 453(7193), 379–382, doi:10.1038/nature06949, 2008.
- 562 McKay, R., Naish, T., Powell, R., Barrett, P., Scherer, R., Talarico, F., Kyle, P., Monien,
563 D., Kuhn, G., Jackolski, C. and Williams, T.: Pleistocene variability of Antarctic Ice
564 Sheet extent in the Ross Embayment, *Quat. Sci. Rev.*, 34, 93–112,
565 doi:10.1016/j.quascirev.2011.12.012, 2012.
- 566 Melles, M., Brigham-Grette, J., Minyuk, P. S., Nowaczyk, N. R., Wennrich, V.,
567 DeConto, R. M., Anderson, P. M., Andreev, A. A., Coletti, A., Cook, T. L., Haltia-Hovi,
568 E., Kukkonen, M., Lozhkin, A. V., Rosen, P., Tarasov, P., Vogel, H. and Wagner, B.: 2.8
569 Million Years of Arctic Climate Change from Lake El'gygytgyn, NE Russia, *Science*,
570 337(6092), 315–320, doi:10.1126/science.1222135, 2012.
- 571 Miller, G. H., Alley, R. B., Brigham-Grette, J., Fitzpatrick, J. J., Polyak, L., Serreze, M.
572 C. and White, J. W. C.: Arctic amplification: can the past constrain the future?, *Quat. Sci.*
573 *Rev.*, 29(15-16), 1779–1790, doi:10.1016/j.quascirev.2010.02.008, 2010a.

574 Miller, G. H., Brigham-Grette, J., Alley, R. B., Anderson, L., Bauch, H. A., Douglas, M.
575 S. V., Edwards, M. E., Elias, S. A., Finney, B. P., Fitzpatrick, J. J., Funder, S. V.,
576 Herbert, T. D., Hinzman, L. D., Kaufman, D. S., MacDonald, G. M., Polyak, L., Robock,
577 A., Serreze, M. C., Smol, J. P., Spielhagen, R., White, J. W. C., Wolfe, A. P. and Wolff,
578 E. W.: Temperature and precipitation history of the Arctic, *Spec. Theme Arct.*
579 *Palaeoclim. Synth.* PP 1674-1790, 29(15–16), 1679–1715,
580 doi:10.1016/j.quascirev.2010.03.001, 2010b.

581 Otto-Bliesner, B. L., Marshall, S. J., Overpeck, J. T., Miller, G. H., Hu, A. and CAPE
582 Last Interglacial Project Members: Simulating Arctic Climate Warmth and Icefield
583 Retreat in the Last Interglaciation, *Science*, 311(5768), 1751–1753,
584 doi:10.1126/science.1120808, 2006.

585 Pollard, D. and DeConto, R. M.: Modelling West Antarctic ice sheet growth and collapse
586 through the past five million years, *Nature*, 458(7236), 329–332,
587 doi:10.1038/nature07809, 2009.

588 Polyak, L., Alley, R. B., Andrews, J. T., Brigham-Grette, J., Cronin, T. M., Darby, D. A.,
589 Dyke, A. S., Fitzpatrick, J. J., Funder, S., Holland, M., Jennings, A. E., Miller, G. H.,
590 O'Regan, M., Saville, J., Serreze, M., St. John, K., White, J. W. C. and Wolff, E.:
591 History of sea ice in the Arctic, *Spec. Theme Arct. Palaeoclim. Synth.* PP 1674-1790,
592 29(15–16), 1757–1778, doi:10.1016/j.quascirev.2010.02.010, 2010.

593 Prokopenko, A. A., Bezrukova, E. V., Khursevich, G. K., Solotchina, E. P., Kuzmin, M.
594 I. and Tarasov, P. E.: Climate in Continental Interior Asia During the Longest Interglacial
595 of the Past 500000 Years: The New MIS 11 Records from Lake Baikal, SE Siberia, *Clim*
596 *Past*, 6, 31–48, 2010.

597 Quiquet, A., Ritz, C., Punge, H. J. and Salas y Mélia, D.: Greenland ice sheet
598 contribution to sea level rise during the last interglacial period: a modelling study driven
599 and constrained by ice core data, *Clim Past*, 9(1), 353–366, doi:10.5194/cp-9-353-2013,
600 2013.

601 Raymo, M. E. and Mitrovica, J. X.: Collapse of polar ice sheets during the stage 11
602 interglacial, *Nature*, 483(7390), 453–456, doi:10.1038/nature10891, 2012.

603 Robinson, A., Calov, R. and Ganopolski, A.: Greenland ice sheet model parameters
604 constrained using simulations of the Eemian Interglacial, *Clim Past*, 7(2), 381–396,
605 doi:10.5194/cp-7-381-2011, 2011.

606 Scherer, R. P., Bohaty, S. M., Dunbar, R. B., Esper, O., Flores, J.-A., Gersonde, R.,
607 Harwood, D. M., Roberts, A. P. and Taviani, M.: Antarctic records of precession-paced
608 insolation-driven warming during early Pleistocene Marine Isotope Stage 31, *Geophys.*
609 *Res. Lett.*, 35(3), doi:10.1029/2007GL032254, 2008.

610 Schilt, A., Baumgartner, M., Blunier, T., Schwander, J., Spahni, R., Fischer, H. and
611 Stocker, T. F.: Glacial–interglacial and millennial-scale variations in the atmospheric

612 nitrous oxide concentration during the last 800,000 years, *Quat. Sci. Rev.*, 29(1-2), 182–
613 192, doi:10.1016/j.quascirev.2009.03.011, 2010.

614 Serreze, M. C. and Hurst, C. M.: Representation of Mean Arctic Precipitation from
615 NCEP–NCAR and ERA Reanalyses, *J. Clim.*, 13(1), 182–201, doi:10.1175/1520-
616 0442(2000)013<0182:ROMAPF>2.0.CO;2, 2000.

617 Stocker, T. F., Qin, D., Plattner, G.-K., Tignor, M., Allen, S. K., Boschung, J., Nauels,
618 A., Xia, Y., Bex, V. and Midgley (eds.), P. .: IPCC,2013: Climate Change 2013: The
619 Physical Science Basis. Contribution of Working Group I to the Fifth Assessment Report
620 of the Intergovernmental Panel on Climate Change, Camb. Univ. Press Camb. UK N. Y.
621 NY USA, 1535 pp, doi:10.1017/CBO9781107415324, 2013.

622 Stone, E. J., Lunt, D. J., Annan, J. D. and Hargreaves, J. C.: Quantification of the
623 Greenland ice sheet contribution to Last Interglacial sea level rise, *Clim Past*, 9(2), 621–
624 639, doi:10.5194/cp-9-621-2013, 2013.

625 Tarasov, P. E., Nakagawa, T., Demske, D., Österle, H., Igarashi, Y., Kitagawa, J.,
626 Mokhova, L., Bazarova, V., Okuda, M., Gotanda, K., Miyoshi, N., Fujiki, T., Takemura,
627 K., Yonenobu, H. and Fleck, A.: Progress in the reconstruction of Quaternary climate
628 dynamics in the Northwest Pacific: A new modern analogue reference dataset and its
629 application to the 430-kyr pollen record from Lake Biwa, *Earth-Sci. Rev.*, 108(1-2), 64–
630 79, doi:10.1016/j.earscirev.2011.06.002, 2011.

631 Thompson, S. L. and Pollard, D.: Greenland and Antarctic mass balances for present and
632 doubled atmospheric CO₂ from the GENESIS version-2 global climate model, *J. Clim.*,
633 10(5), 871–900, 1997.

634 De Vernal, A. and Hillaire-Marcel, C.: Natural Variability of Greenland Climate,
635 Vegetation, and Ice Volume During the Past Million Years, *Science*, 320(5883), 1622–
636 1625, doi:10.1126/science.1153929, 2008.

637 Viereck, L. A. and Little Jr, E. L.: *Atlas of United States Trees, Volume 2: Alaska Trees
638 and Common Shrubs.*, 1975.

639 Willerslev, E., Cappellini, E., Boomsma, W., Nielsen, R., Hebsgaard, M. B., Brand, T.
640 B., Hofreiter, M., Bunce, M., Poinar, H. N., Dahl-Jensen, D., Johnsen, S., Steffensen, J.
641 P., Bennike, O., Schwenninger, J.-L., Nathan, R., Armitage, S., de Hoog, C.-J., Alfimov,
642 V., Christl, M., Beer, J., Muscheler, R., Barker, J., Sharp, M., Penkman, K. E. H., Haile,
643 J., Taberlet, P., Gilbert, M. T. P., Casoli, A., Campani, E. and Collins, M. J.: Ancient
644 Biomolecules from Deep Ice Cores Reveal a Forested Southern Greenland, *Science*,
645 317(5834), 111–114, doi:10.1126/science.1141758, 2007.

646 Woodgate, R. A., Weingartner, T. and Lindsay, R.: The 2007 Bering Strait oceanic heat
647 flux and anomalous Arctic sea-ice retreat, *Geophys. Res. Lett.*, 37(1), n/a–n/a,
648 doi:10.1029/2009GL041621, 2010.

649 Yin, Q. Z. and Berger, A.: Individual contribution of insolation and CO₂ to the
650 interglacial climates of the past 800,000 years, *Clim. Dyn.*, 38(3-4), 709–724,
651 doi:10.1007/s00382-011-1013-5, 2011.

652

653

654

655

656

657

658

659

660

661

662

663

664

665

666

667

668

669

670

671

672

673

674

675

676

677

678

679

680

681

682

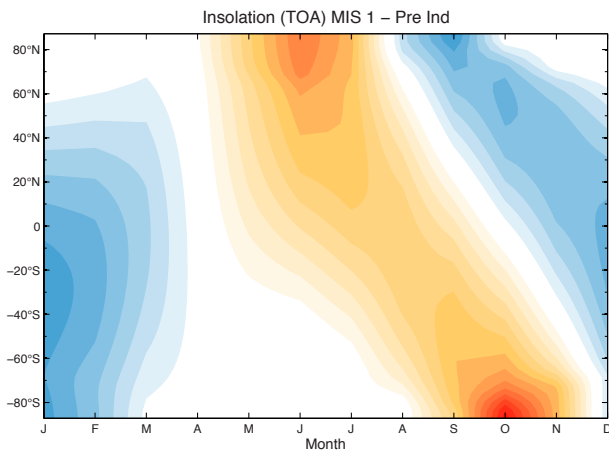
683

684 **Figures:**

685

686

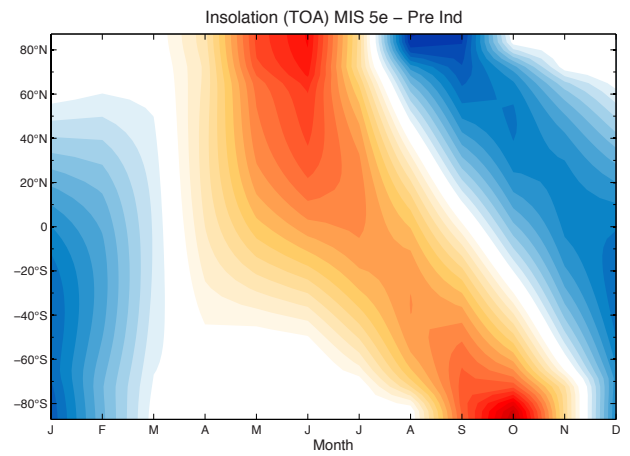
A



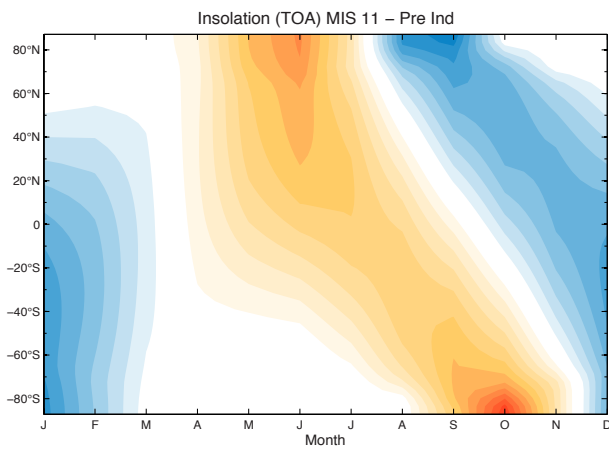
B

687

688

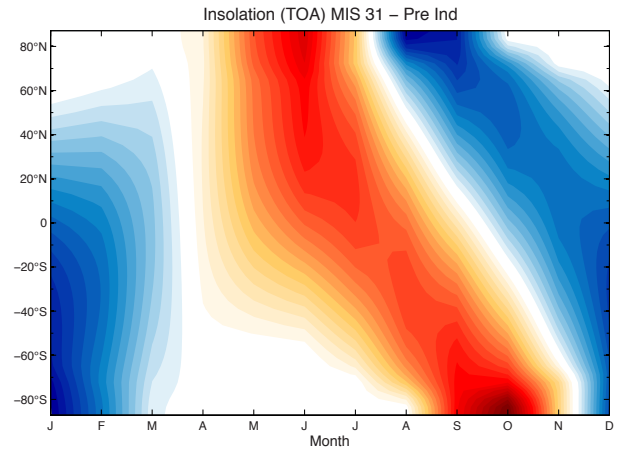


C



D

689



690

691

692

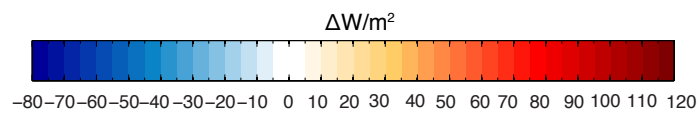


Figure 1: Monthly insolation anomalies at the top of the atmosphere for the interglacial intervals modeled here [W/m^2]. **A MIS-1 anomalies with respect to modern orbit, **B** MIS-5e anomalies with respect to modern orbit, **C** MIS-11c anomalies with respect to modern orbit and **D** MIS-31 anomalies with respect to modern orbit.**

693

694

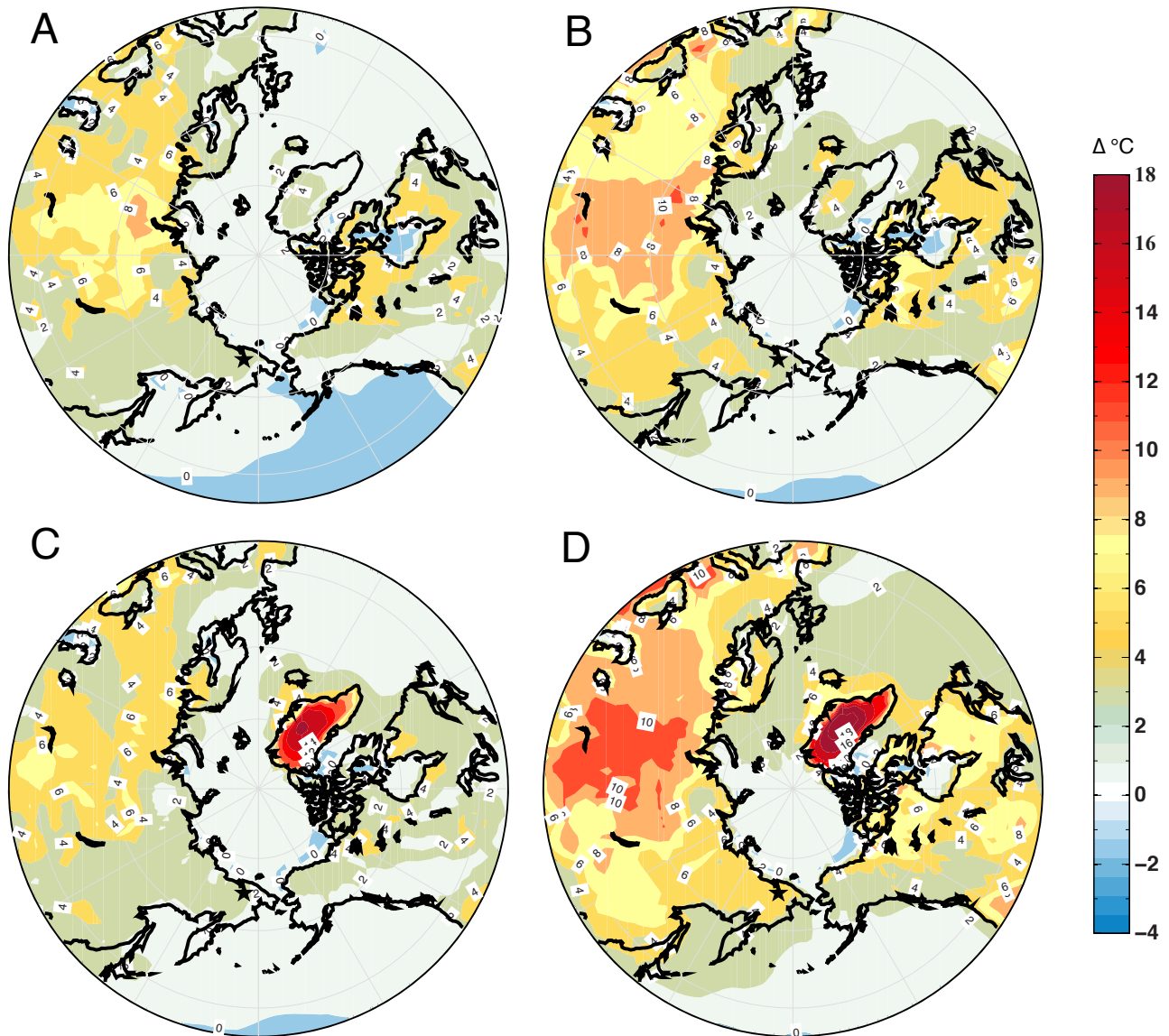


Figure 2: Simulated interglacial anomalies (2-meter annual air temperature in °C) relative to pre-industrial temperatures. A MIS-1 (9 ka orbit and GHGs), B MIS-5e (127 ka orbit and GHGs), C MIS-11c (409 ka orbit and GHGs, and no Greenland Ice Sheet), D MIS-31 (1072 ka orbit and GHGs, and no Greenland Ice Sheet). The location of Lake El'gygytyn (black star) is shown near the bottom of each panel. Areas of no shading (white) roughly correspond to no change that is statistically significant at the 95% confidence interval.

700
701
702

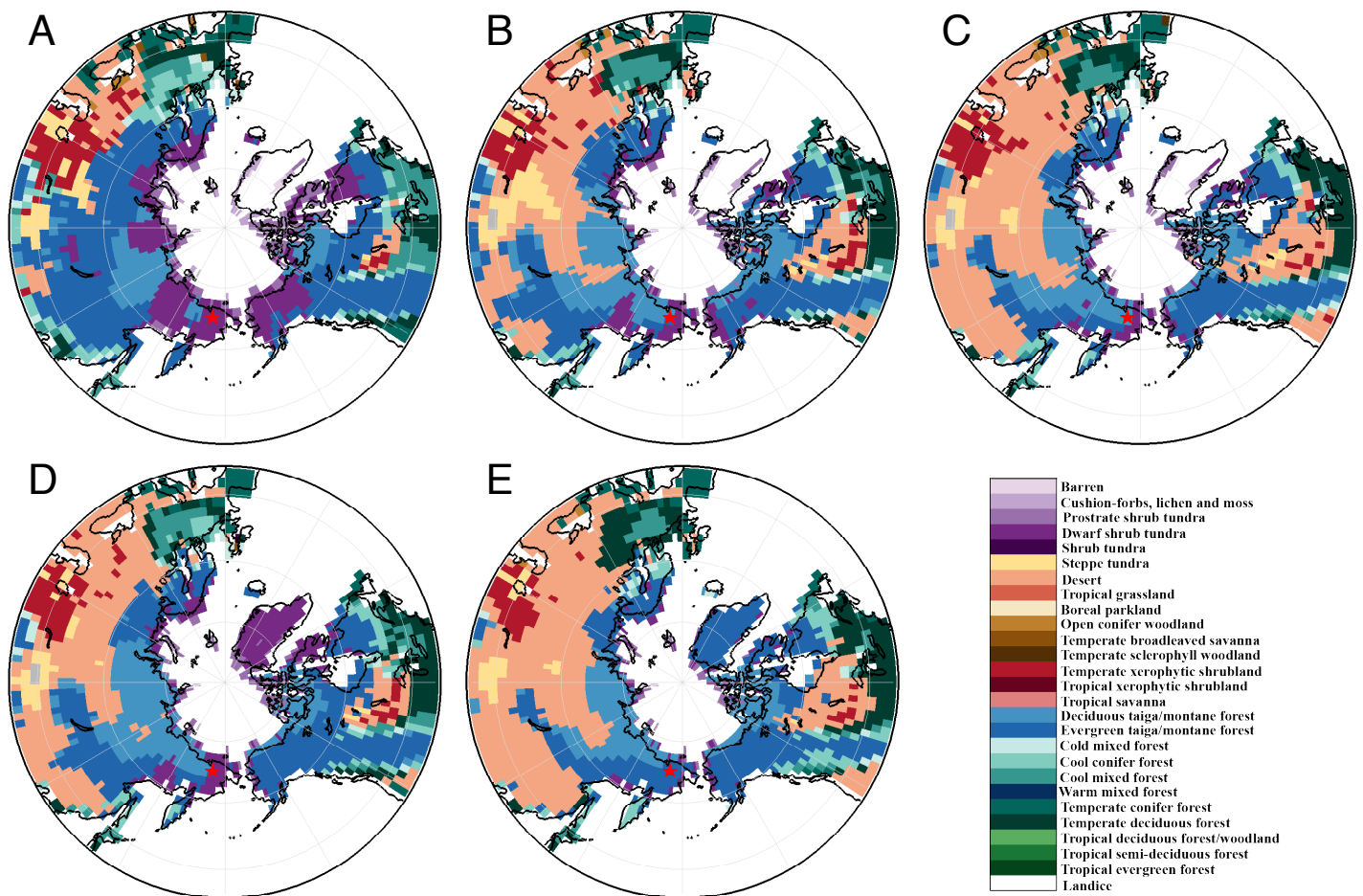


Figure 3: Distribution of interglacial vegetation simulated by the BIOME4 interactive vegetation model coupled to the GCM. A Pre-Industrial vegetation corresponding to modern summer anomalies, **B** MIS-1 (9 ka), **C** MIS-5e vegetation, **D** MIS11NG vegetation and **E** MIS-31 (no GIS) vegetation. The location of Lake E is shown near the bottom of each figure with a red star. Note the poleward advancement of evergreen and needle-leaf trees around the lake during each interglacial and the replacement of shrub tundra to taiga forest.

703
704
705
706
707
708
709
710
711
712

713
714
715
716
717
718
719
720
721
722
723
724
725
726
727
728
729
730
731
732
733
734
735
736
737
738
739
740
741
742
743
744
745
746
747
748
749
750
751
752
753
754
755
756
757
758
759
760
761
762
763

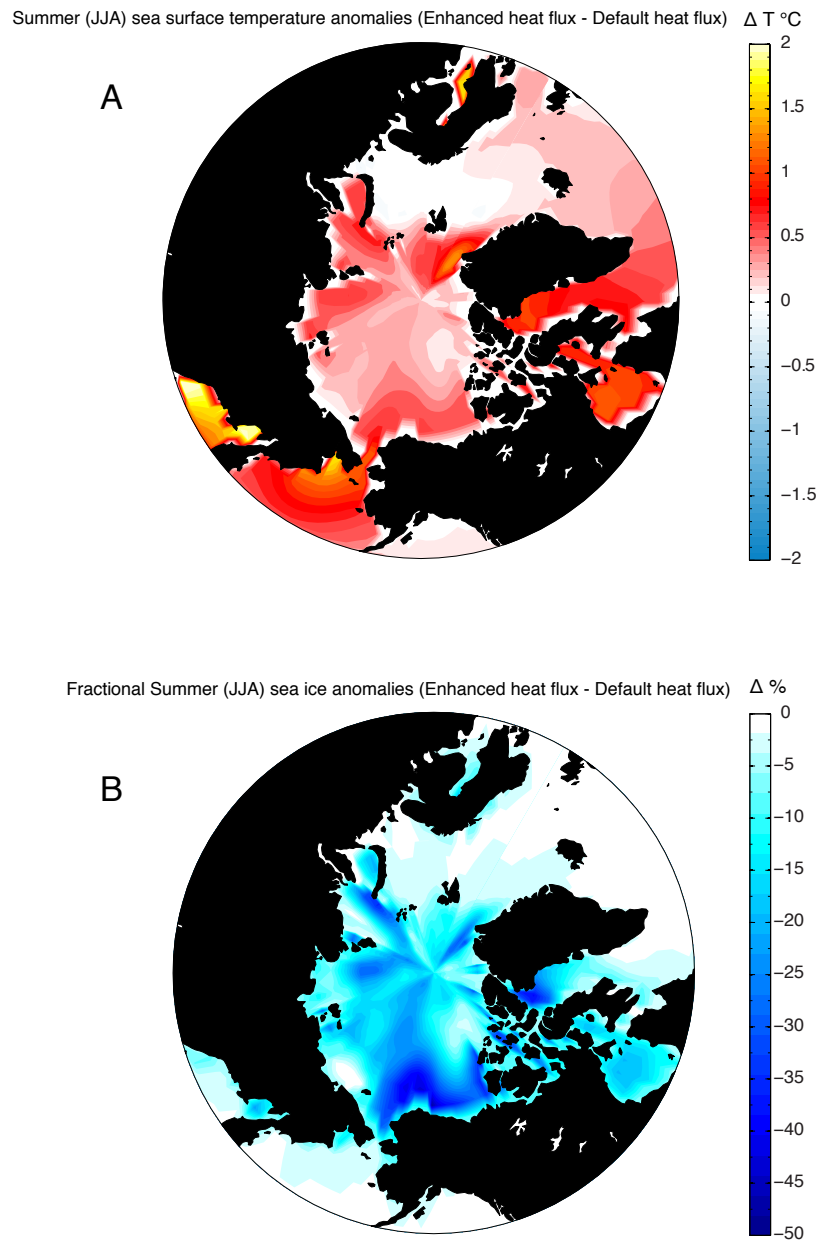


Figure 4: Model simulated (MIS11NG) Summer sea surface temperature and sea ice anomalies caused by enhanced oceanic heat flux (+8 W/m²) at 409 ka. A Summer (JJA) sea surface temperature change with respect to default heat flux simulation (T °C) and B Summer (JJA) sea ice fraction anomalies (%) with respect to default heat flux simulation. With +8 W/m² of sub-sea ice heat flux convergence, Arctic Ocean SSTs rise > 0.5 °C and sea ice fraction decreases 25-50% in most areas.

764
 765
 766
 767
 768
 769
 770
 771
 772
 773
 774
 775
 776
 777

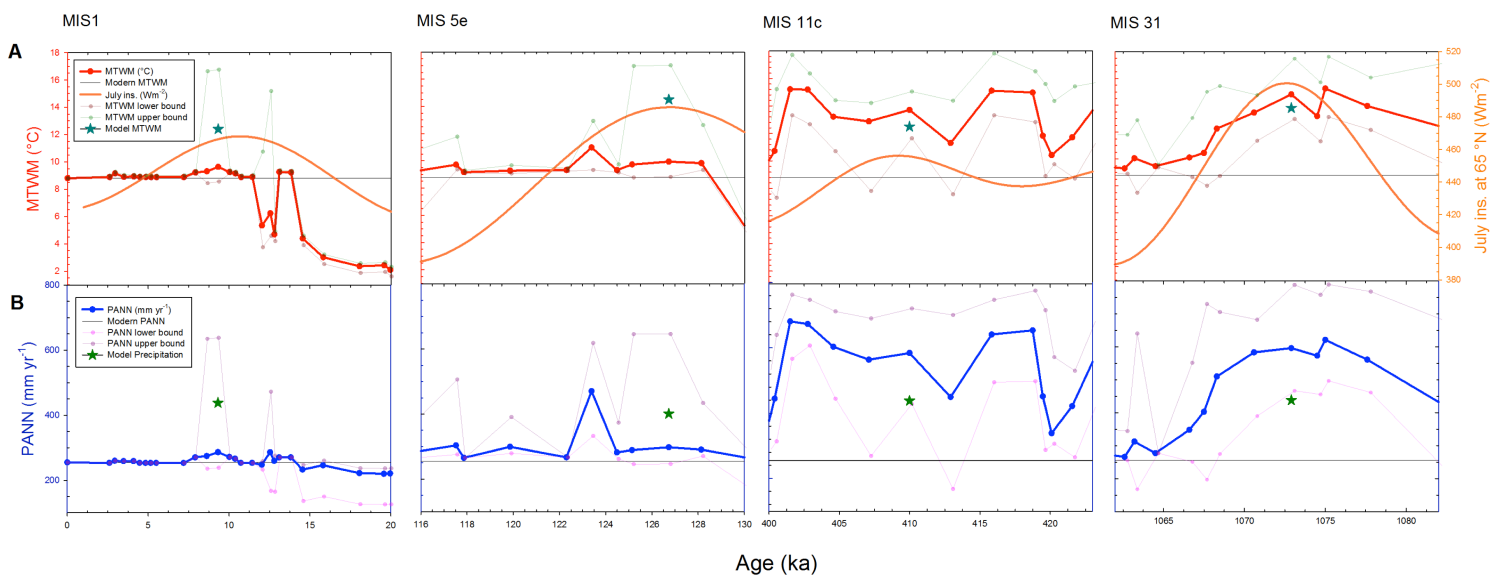


Figure 5: (A and B) A Reconstructed MTWM and B PANN from *Melles et al., 2012*. Transparent data above and below the **bolded lines are upper and lower limits of each data point calculated from a best modern analogue technique (MAT) function. The dark cyan (A) and dark green (B) stars denote results from the GCM simulations with respect to MTWM and PANN.**

778
 779
 780
 781
 782
 783
 784
 785
 786
 787
 788
 789
 790
 791

792
793
794
795
796
797
798
799
800
801
802
803
804

Table 1: Overview of interglacial simulations performed during this study. Orbital configurations (**Berger, 1978**) and greenhouse gas (GHG) concentrations (**Honisch et al., 2009; Loulergue et al., 2008; Lüthi et al., 2008; Schilt et al., 2010**). Modern GHG concentrations are taken from 1950 AD; obliquity is given in degrees and precession is Ω in degrees.

Age	Run description	CO ₂ (ppmv)	CH ₄ (ppbv)	N ₂ O (ppbv)	Eccentricity	Obliquity (°)	Precession (Ω , °)
1850 AD	pre-industrial simulation with pre-industrial GHG concentrations	280	801	289	0.01671	23.438	101.37
9 ka	MIS 1 - with (modern) GIS	~260	~611	~263	0.01920	24.229	310.32
127 ka	MIS 5e - with (modern) GIS	287	724	262	0.03938	24.040	272.92
409 ka	MIS 11c - with (modern) GIS	285	713	285	0.01932	23.781	265.34
409 ka	MIS 11c - no GIS	285	713	285	0.01932	23.781	265.34
409 ka	MIS 11c - no GIS + 10 Wm ⁻² increase of heat flux under sea ice	285	713	285	0.01932	23.781	265.34
1072 ka	MIS 31 - with no GIS	325	800	288	0.05597	23.898	289.79

805
806
807
808
809
810
811
812
813
814
815
816
817
818
819
820
821
822
823
824
825
826

827
828
829
830
831
832

Table 2: List of GCM simulations with corresponding variables at the grid cell location of Lake E.

Run	Pre-industrial	MIS 1-with GIS	MIS 5e-with GIS	MIS 11c-with GIS	MIS 11c-no GIS	MIS 11c-noGIS-10Wm ⁻²	MIS 31-without GIS
Lake-E							
MAAT (°C)	-12	-12	-12.4	-11.5	-12.5	-10.5	-10.4
Summer Temp (JJA; °C)	8	9.6	10.5	10	10.2	10.5	11.8
MTWM (July, °C)	10.3	12.4	14.5	12.2	12.5	13.2	13.8
PANN (mm yr ⁻¹)	438	438	401	475	438	475	438

833
834
835
836
837